Microchimica Acta
https://doi.org/10.1007/s00604-018-2693-x

ORIGINAL PAPER

Electrochemiluminescence based detection of microRNA by applying an amplification strategy and Hg(II)-triggered disassembly of a metal organic frameworks functionalized with ruthenium(II)tris(bipyridine)

Yannan Jian[1,2] · He Wang[1] · Feifei Lan[1] · Linlin Liang[1] · Na Ren[1] · Haiyun Liu[1] · Shenguang Ge[1] · Jinghua Yu[1,2]

Received: 25 October 2017 / Accepted: 18 January 2018

Abstract

An electrochemiluminescence (ECL) biosensor is described for the detection of microRNA (miRNA-155) based on tris(bipyridine)ruthenium(II) functionalized metal organic framework (RuMOF) materials. The material was prepared by a solvothermal method and was found to be stable even in acidic solution. However, it is selectively and sensitively disassembled by Hg(II) ions, resulting in the release of large quantities of Ru(II)$(bpy)_3$ ions, which produces a strong ECL signal. In view of the ion-selective disassembly and release and strand displacement process, an ultrasensitive ECL sensing method was established for detection of microRNAs. In the presence of the target, the hairpin structure of H1 can open and hybridize with the hairpin probe H2 to form a more stable H1-H2 duplex structure than the H1-target hybrid. The target of hybridization to H1 was immediately freed from the structure and the released target re-entered the new hairpin assembly target recovery process. The remaining H2 single fragment can bind to the I-RuMOFs-conjugates. The more hairpin probes H1, the more I-RuMOFs-conjugates load the DNA fragments, leading to the signal amplification. The method works in the 0.8 f. to 1.0 nM miRNA-155 concentration range and has a detection limit of 0.3 fM. The assay is sensitive, fairly specific and remarkably stable. In our perception, it offers an attractive tool for the sensitive detection of microRNAs in clinical samples.

Keywords Ion-selective disassembly · Strand displacement process · Signal amplification

Introduction

MicroRNAs (miRNAs), a large family of endogenous and small (~18–25 nucleotides in length) noncoding RNAs, has enormous potential to become new biological marker for diagnosis. They also are of interest in drug research and development, which might provide a promising means for the treatment of human disease [1, 2]. With the purpose of accurately detecting miRNAs, extremely sensitive and quantitative detection of miRNAs is essential, mainly including northern analysis, microarray analysis, quantitative real-time polymerase chain reaction [3, 4]. As an alternative to the conventional detection procedure, electrochemiluminescence (ECL) assay has revealed bright prospect in fast, selective, and sensitive detection of analyte [5]. Design a kind of practical ECL biosensors by applying ECL technology for the detection of miRNAs is necessary. To enhance the sensitivity of detection, a large number of amplification strategies were properly introduced [6, 7], which is because miRNAs are at the attomolar to femtomolar level in biological samples [8]. The signal amplification for ECL assay is a key issue for the sensitive biosensor. Signal amplification strategies reported so far mainly include metal and semiconductor nanomaterials label [9], catalytically deposited nanoparticles [10], metal nanocarriers [11], multiple enzyme particles [12] and dual amplification [13]. Of course, some works have reported the ECL detection by making use of tris(bipyridine)ruthenium ($Ru(bpy)_3^{2+}$) [14, 15]. However, it is never reported concerning the sensitive detection of miRNAs by using ECL principle of $Ru(bpy)_3^{2+}$ functionalized metal organic frameworks (abbr. RuMOFs).

Electronic supplementary material The online version of this article (https://doi.org/10.1007/s00604-018-2693-x) contains supplementary material, which is available to authorized users.

✉ Haiyun Liu
chm_liuhy@yjn.edu.cn

✉ Shenguang Ge
chm_gesg@163.com

[1] Institute for Advanced Interdisciplinary Research, University of Jinan, Jinan 250022, People's Republic of China

[2] Key Laboratory of Interfacial Reaction & Sensing Analysis in Universities of Shandong, School of Chemistry and Chemical Engineering, University of Jinan, Jinan 250022, People's Republic of China

Published online: 25 January 2018

Nowadays, the fabrication of MOFs has attracted a fervent concern. And a variety of MOFs for storage gases [16], supported catalysts [17], transport and release drugs [18] have been applied so far. As ionic luminescent reagent, $Ru(bpy)_3^{2+}$ has high emission efficiency and has been also successfully applied to the ECL [19]. Thus, $Ru(bpy)_3^{2+}$ was chosen the guest material and wrapped in MOFs to form novel RuMOFs. The carboxyl-modified DNA strand I was immobilized on RuMOFs by acid amine condensation reaction. It was worth pointing out that we took advantage of the Hg^{2+}-triggered release of $Ru(bpy)_3^{2+}$ from RuMOFs. Mercury ions can disassemble MOFs, leading to the guest material was released. Once the mercury ions were added, the guest materials would be released. Thus, this flexible ECL biosensor based on the RuMOFs to measure miRNA-155 was designed.

Gold nanoparticles (Au NPs) with amazing conductivity and large specific surface were frequently used as accelerator for ECL biosensors in order to amplify the signal and enhance the performance of biosensors [20–22]. That was the reason why the glassy carbon electrode (i.e, GCE) was modified with Au NPs. An ideal biosensor for signal amplification and quantitative detection of target was established, which reasonably and availably utilized hairpin assembly target recycling (HTR) process and the high-efficiency release of $Ru(bpy)_3^{2+}$. The designed biosensor can convert the single target miRNA input to large numbers of signal molecule output after cycling amplification, which can improve the amplification efficiency, further enhancing the sensitivity of the biosensor. The biosensor displayed many advantages such as wide linear range and low detection limit. In addition to above advantages, the biosensor provided a promising quantitative detection method of miRNA-155 in the clinical applications. Moreover, the method for preparing luminophore-based nanostructures would have a wider application in bioanalysis due to its simplicity, convenience and effectiveness. Such an ECL biosensor also provided new opportunities for ultrasensitive detection of microRNAs at very low concentrations, and it was expected to provide new possibilities for other biomolecules diagnostics as well as for bioanalysis in general.

Experimental

Reagents

All DNA and RNA sequences were synthesized and purified by Sangon (Shanghai, China, http://www.sangon.com/). Tris(bipyridine) ruthenium (II) ($Ru(bpy)_3^{2+}$, 98%), Zinc nitrate hexahydrate ($Zn(NO_3)_2•6H_2O$) and adenine (99%) were purchased from Alfa Aesar Co. Ltd. (China, https://www.alfa.com/zh-cn/) 4,4′-Biphenyldicarboxylate (BPDC, 97%), chloroauric acid($HAuCl_4$) and (3-aminopropyl)-triethoxysilane (APTES) were acquired from Sigma-Aldrich Chemical Co. (USA, http://www.sigmaaldrich.com/). Tripropylamine (TPA) and 6-mercapto-1-hexanol (MCH) were purchased from Nanoport. Co. Ltd. (Shenzhen, China, http://www.nanotubes.com.cn/). N,N-dimethylformamide (DMF) of analytical purity was purchased from Aladdin Industrial Corporation (China, http://www.diytrade.com/). All chemicals and solvents used here were the analytical grade or above. Ultrapure water was used throughout all experiments and obtained from an Ulupure UPR-II-10 T water-purification system (resistivity≥18.2 MΩ·cm, Ulupure, China, http://www.sdjncc.com/). The sequences of oligonucleotides were presented as below:

I: 5′- COOH- TTA GTC GCT CCT- 3′.

Target (miRNA-155): 5′- UUA AUG CUA AUC GUG AUA GGG GU- 3′.

H1:5′- TAA TCG TGA TAG GGG TAT GGA CAT GGA ACC CCT ATC ACG ATT AGC ATT AAA GA- SH- 3′.

H2: 5′- ATG GAC ATG GAT AAT CGT GAT AGG GGT CCC ATG TCC ATA CCC CTA TGA AGG AGC GAC T- 3′.

noncomplementary DNA (nDNA): 5′- GGT TGG TGT GGT TGG- 3′.

miRNA-101 (nRNA): 5′- UAC AGU ACU GUG AUA ACU GAA- 3′.

single-base difference miRNA (sRNA): 5′- UUA AGG CUA AUC GUG AUA GGG GU- 3′.

The buffers involved were as follows: probe hybridization buffer (pH 7.4), 10 mM Tris-HCl, 1.0 mM ethylenediaminetetraacetic acid (EDTA), 10 mM trichloroethyl phosphate (TCEP), 0.1 M NaCl; DNA immobilization buffer (pH 7.0), 10 mM Tris-HCl, 1.0 mM EDTA, 1.0 M NaCl; miRNA hybridization buffer (pH 8.0), 10 mM Tris-HCl, 1.0 mM EDTA, 0.2 M NaCl, 10 mM $MgCl_2$. 1 × TE buffer (pH 8.0), 10 mM Tris-HCl, 1.0 mM EDTA, was used for dissolving all oligonucleotides.

Apparatus

Scanning electron microscope (SEM) image was obtained using a QUANTA FEG 250 thermal field emission SEM (FEI Co., USA, https://www.fei.com/home/) and the microscope was equipped with an Oxford X-MAX50 energy dispersive spectrometer (EDS) (Oxford, Britain, https://www.oxford-instruments.com/). Transmission electron microscopy (TEM) investigation was performed using JEOL 4000 EX microscope (https://www.jeolusa.com/). TEM system opened at an accelerating voltage of 200 kV. X-ray diffraction (XRD) pattern of the powder samples was collected at room temperature on a Rigaku D/MAX 2200PC diffractometer (China, http://www.ddtdkj.cn/cn/cpzs/). The fluorescence spectra were obtained on a LS-55 spectrofluorometer (P.E. USA, http://www.pe-us.com/). Cyclic voltammetry (CV) and electrochemical impedance spectroscopy (EIS) were

performed with a CHI 660D electrochemical workstation (Shanghai Chenhua Instrument Co., Ltd., China, http://www.chinstr.com/). The ECL measurements were carried out on a MPI-E multifunctional electrochemical and chemiluminescence analytical system (Xi'an Remax Analytical Instrument Ltd. Co., China, http://remax.testmart.cn/) biased at 800 V.

Fabrication of RuMOFs

The Fabrication of RuMOFs was similar to previous work with major modifications and a detailed procedure as described below [23]. Adenine (0.2 mM), BPDC (0.4 mM), $Zn(NO_3)_2{\cdot}6H_2O$ (0.45 mM) and $Ru(bpy)_3Cl_2{\cdot}6H_2O$ (0.35 mM) were added to the mixed solvent, which consisted of HNO_3 (2 mM), DMF (20 mL) and water (3 mL). Subsequently, the mixed solution was treated with a solvothermal method at 110 °C for 12 h. Then, the rod-like crystals were obtained by successive centrifugation and the precipitate was repeatedly washed with DMF and H_2O for three times. Finally, the obtained RuMOFs were dissolved in 6 ml of PBS (0.1 M, pH 7.0) for subsequent experiments.

Synthesis of I-RuMOFs-conjugates

The material needs to be treated prior to carrying out the linker moiety. For the preparation of I-RuMOFs-conjugates, 4 mL of RuMOFs was dispersed in 2 mL of ethanol and treated with 0.4 mL of APTES. After stirring for 6 h, the suspension was centrifuged and washed with ethanol repeatedly for four times and the amino-functionalized RuMOFs was obtained. First of all, added 150 μL of carboxyl-modified I (3 μM) that was dissolved with sterilized water to 1 mL of the amino-functionalized RuMOFs, shaking the mixed solution gently at 10 °C overnight. Afterwards, the pure I-RuMOFs-conjugates were obtained by centrifuging, washing three times with water, and recentrifuging, followed by dispersal in Tris-HCl buffer (10 mM) and stored at 4 °C before use.

Fabrication of the miRNA-155 biosensor

Scheme 1 demonstrated the fabrication process of the ECL biosensor. Prior to compositing the miRNA biosensor, a GCE (diameter of 3 mm) was polished with 0.3 and 0.05 μm α-Al_2O_3 powder to obtain a smooth surface. After successive sonication in 1:1 nitric acid and acetone for 20 min, the electrode was rinsed with H_2O and allowed to dry at room temperature. After that, the cleaned electrode was immersed in 5 mL of 1% $HAuCl_4$ solution, and treated in −0.2 V for 40 s for the electrodeposition of the Au NPs film. Then the modified electrode was rinsed thoroughly with water and dried under a stream of N_2. Whereafter, the modified electrode was incubated with 10 μL of thiol-modified H1 (2 μM) for 16 h so that H1 was stably fixed on the modified electrode by Au-S covalent bond. After cleaning with ultrapure water, 10 μL of MCH (1.0 mM) was dropped onto the surface of modified electrode in order to prevent nonspecific absorption by blocking the modified electrode. After that, the modified electrode was incubated under the condition of 6 μL of H2 (4 μM) and 6 μL of target miRNA-155 (3 μM) for 2 h at 25 °C. Ultimately, 10 μL of I-RuMOFs-conjugates were added to the surface of electrode for 2 h at 25 °C. It was to be noted that after each modification was completed, remember to rinse with ultrapure water.

Results and discussions

Amplification strategy

An ultrasensitive ECL biosensor for miRNA-155 detection was developed, which based on the superior characteristic of $Ru(bpy)_3^{2+}$ functionalized MOFs and hairpin assembly target recycling process for signal amplification. The capture probe H1 was fixed on the Au NPs/GCE by Au-S covalent bond. Furthermore, hairpin structure of H1 opened as soon as target appeared. Under the participation of hairpin probe H2, H2 replaced and liberated the target on account of the superior stability and length of H1-H2 duplex structure than H1-target hybrid. So the target which was hybridized with H1 can liberate immediately from the structure. The released target was reentered the new hairpin assembly target recycling process and vast H1-H2 duplex structure was generated after the hairpin assembly target recycling process, which tremendously promoted the signal amplification. Furthermore, remaining single fragments of H2 can combine with DNA strand I. The more hairpin probe H1 exited, the more loading of I-RuMOFs-conjugates toward DNA fragments. Finally, the signal amplification was implemented in the way, the quantitative determination of miRNA-155 would be realized. The method has the advantage of maneuverability, thus it will be flexibly applied.

Characterization of RuMOFs

To demonstrate the desirable preparation of RuMOFs, SEM and TEM were used to verify the morphology of RuMOFs. As shown in Fig. 1a, SEM image of RuMOFs suggested that the RuMOFs distinctly owned monodispersity and rod-shaped structure with a length of 115 ± 10 nm and a diameter of 45 ± 5 nm ($n = 5$). TEM image further showed the porosity of the synthesized RuMOFs in Fig. 1b. It should be noted that the TEM image was taken from the top view of the rod-shaped RuMOFs. As shown in Fig. S1, the elemental composition of RuMOFs was analyzed with EDS. The EDS analysis suggested that the sample consisted of Ru and Zn elements,

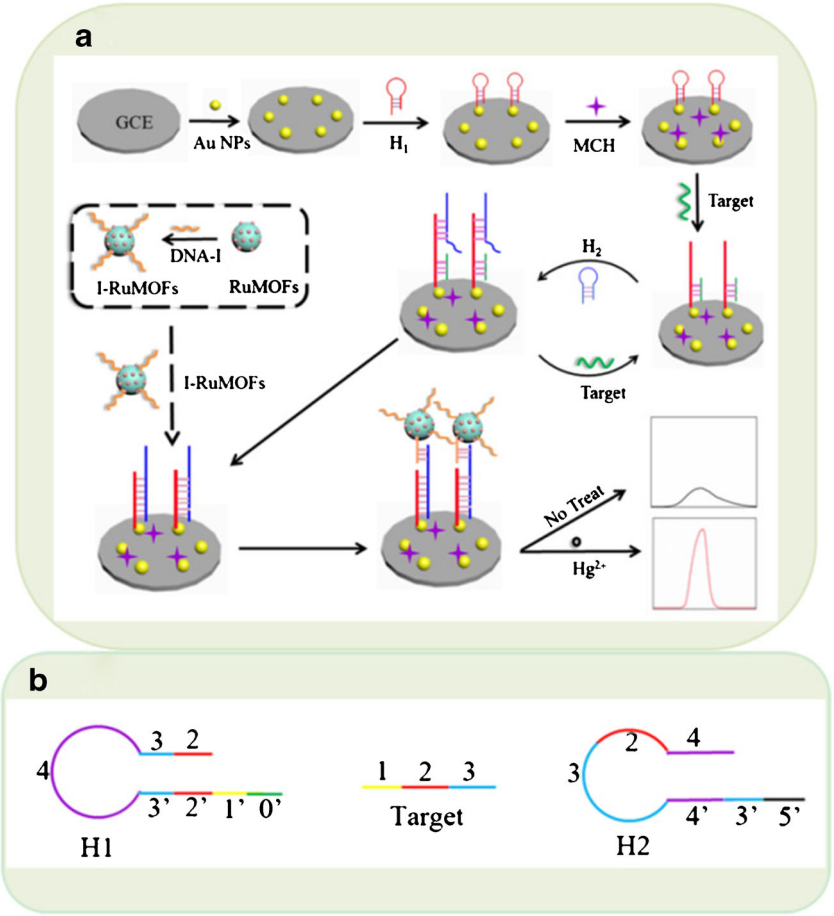

Scheme 1 **a** Schematic representation for detection of miRNA-155 and the strategy of signal amplification (GCE: glassy carbon electrode; Au NPs: Au nanoparticles; H1: capture hairpin probe; MCH: 6-mercapto-1-hexanol; H2: hairpin DNA; I-RuMOFs: tris(bipyridine)ruthenium(II) functionalized metal organic framework materials modified by DNA strand-I); **b** Structure of H1, target and H2 (base pairing complementary parts: 1–1′, 2–2′, 3–3′, 4–4′)

which was further demonstrated that RuMOFs has been synthesized successfully. Guest molecule, $Ru(bpy)_3^{2+}$, was packaged into the frameworks and inserted into the pores of MOFs. The comparison of XRD pattern of RuMOF (see red line in Fig. 1d) with that of their precursor MOF (i.e., bio-MOF-1) (see green line in Fig. 1d) indicates that the functionalization with $Ru(bpy)_3^{2+}$ does not impact the crystalline integrity of bio-MOF-1.

Ion- selective disassembly of RuMOFs

To detect the release of $Ru(bpy)_3^{2+}$ from RuMOFs after the addition of Hg^{2+}, the corresponding characterizations were as follows. As shown in Fig. 2a, the solution supernatant was almost colorless and only gave out a feebly red light at the bottom before the addition of Hg^{2+} (Fig. 2A–a). After the addition of Hg^{2+}, Hg^{2+} triggered the the release of $Ru(bpy)_3^{2+}$ from of RuMOFs, resulting in lots of luminescent ions dispersed into the supernatant. The fluorescence intensity of the system gradually increased with increasing concentration of released $Ru(bpy)_3^{2+}$. So, the system appeared bright red entirely in Fig. 2A-b. This vivid comparison of fluorescence intensity reasonably confirmed our conclusion.

Figure 2b indicated the fluorescence emission intensity obtained from the RuMOFs in the absence and presence of 100 μM Hg^{2+}. From curve a to curve b, fluorescence emission

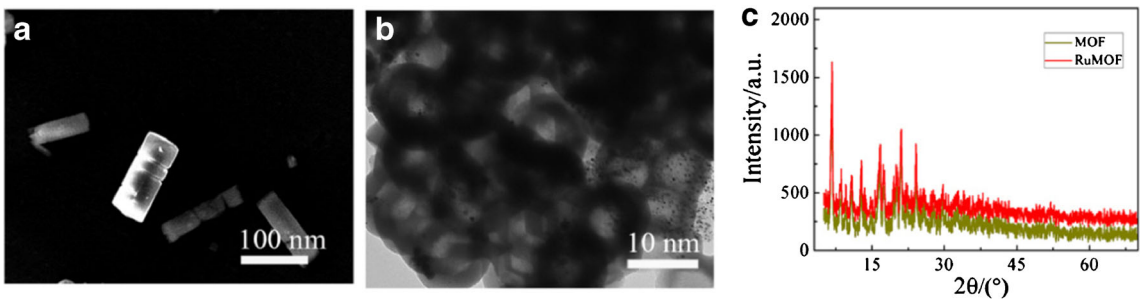

Fig. 1 **a** SEM image of RuMOFs; **b** TEM image of RuMOFs; **c** XRD patterns of MOF and RuMOF

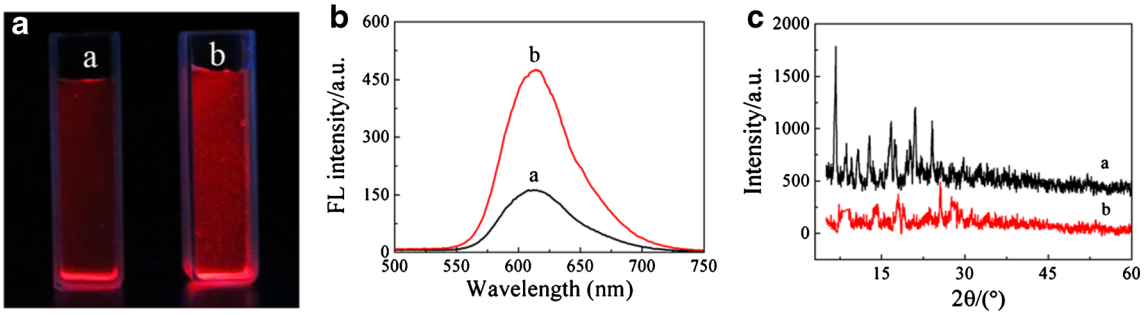

Fig. 2 **a** Provided that 365 nm ultraviolet light, photos of the dilute RuMOFs in the absence (a) and presence (b) of 100 μM Hg^{2+}; **b** fluorescence emission spectra obtained from the dilute RuMOFs in the absence (a) and presence (b) of 100 μM Hg^{2+} (the wavelength of the scanning range: 450 nm~700 nm); **c** XRD patterns of RuMOFs (a), Hg^{2+}-RuMOFs (b)

intensity had an enhanced tendency, that's owing to the rapid and efficient decomposition of Hg^{2+} to the rod-shaped MOFs. The MOF disassembly hypothesis was confirmed by XRD experiment. XRD patterns showed that the characteristic XRD patterns of MOFs (curve a in Fig. 2c) completely disappear after the interaction of RuMOFs with Hg^{2+} (curve b in Fig. 2c). This showed RuMOFs were disassembled.

According to intuitionistic and convenient fluorescence images, gradual transformation of fluorescence intensity was intuitively understood and verified. The fluorescence image of 0 s after adding Hg^{2+} not only presented the features of individuality and dispersity, but also showed a relatively red fluorescence in Fig. 3a. Figure 3b showed the fluorescence intensity transformed weaker after 15 s. Afterwards, fluorescence intensity gradualy weakened in Fig. 3c. As the response continued, the fluorescence was largely weakened when RuMOFs was entirely disintegrated by Hg^{2+} as well as imaged areas turned dark, luminous ions were totally released (Fig. 3d). The cause of the above phenomenon (C and D) was that Hg^{2+} reacted with the guest material-$Ru(bpy)_3^{2+}$. The reaction between Hg^{2+} and RuMOFs was continuous until completed, so the quantity of luminescent ion-$Ru(bpy)_3^{2+}$ can decrease significantly and the fluorescence intensity can greatly reduced as well. Overall, these images can adequately verify that the Hg^{2+} can trigger the decomposition of RuMOFs.

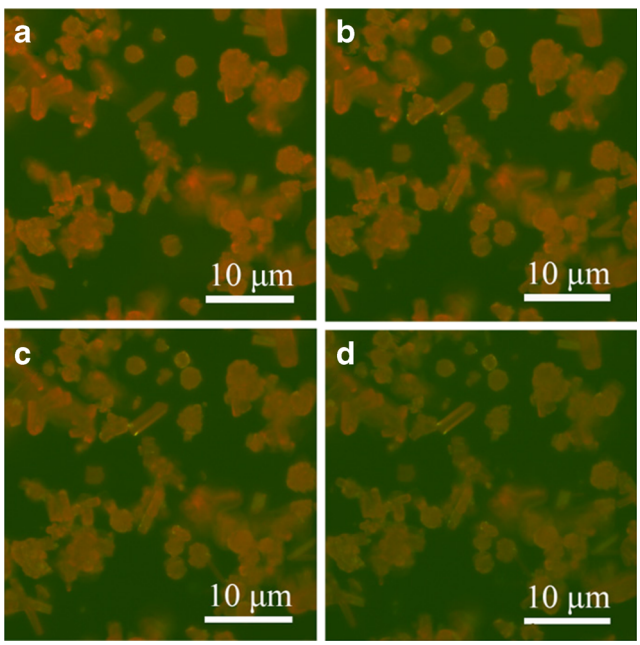

Fig. 3 Fluorescence microscopic images obtained for the Hg^{2+} (10 μM) promoted release of $Ru(bpy)_3^{2+}$ from RuMOFs, which were taken at 0 s (**a**); 15 s (**b**); 30 s (**c**); 45 s (**d**). The excitation wavelength is 425 nm

It is well-known that most MOFs can strongly adsorb some metal ions; however, unlike the classic MOFs, the RuMOF can be selectively disassembled by Hg^{2+} and release luminol ions ($Ru(bpy)_3^{2+}$). As shown in Fig. S2, fluorescence emission spectra was obtained by adding 9 commonly existing H^+ and metal ions, including H^+, Li^+, Mg^{2+}, Ca^{2+}, Pd^{2+}, Mn^{2+}, Fe^{2+}, Fe^{3+} and Hg^{2+} into the dilute RuMOFs. After adding 100 μM of above cations into the RuMOFs, only Hg^{2+} can trigger the release of the luminescent ion (i.e., $Ru(bpy)_3^{2+}$) into the supernatant, whereas no release from the RuMOFs was found in pure water, acid solution (containing H^+), or solutions of other metal ions. These experimental results showed an extremely selective interaction between Hg^{2+} and the RuMOFs.

Mechanism of the proposed ECL biosensor

As can be seen in Scheme 1, the principle of ECL biosensor based on signal amplification strategy by target recycling [24, 25] and ECL behavior of RuMOFs were described clearly in order to detect miRNA-155. At the beginning, 3′-thiol-modified hairpin probe H1 was stably fixed on the surface of Au NPs-modified GCE through Au-S bond. Subsequently, the attended target would hybridize with probe H1 because of complementary base pairing by opening the hairpin structure of H1 and form double-stranded DNA. With the introduction of H2, the exposed sequence of H1 can match with another hairpin probe H2 through branch migration process [26–28]. H2 would replace and liberate the target when it hybridized to H1 on account of the superior stability and length of H1-H2 duplex structure than H1-Target hybrids. Hairpin DNA H1 and H2 can maintain a stable stem structure and not

automatically hybridize with each other provided that shortage of target. Released target continued to be utilized and continuously participated in the next HTR process, increasingly producing remaining single DNA fragments of H2. The generated DNA fragments became available for hybridizing to DNA strand I that was functionalized by RuMOFs. With the quantitative addition of Hg^{2+}, ECL behavior of RuMOFs was detected by ECL detection system. The ECL intensity varies with the concentration of miRNA-155. Hence, quantitative detection of miRNA-155 would be realized deftly.

Performance of the proposed ECL biosensor

In ECL measurements, a mixed solution in phosphate buffered saline (PBS, 0.1 M, pH 7.0) containing TPA (1.0×10^{-3} M) (1:2) was used and the potential was cycled within the window from 0 to 1.25 V with a scan rate of 200 mV·S^{-1}. Under the optimum conditions, Fig. 4a apparently showed that the ECL intensity of the proposed sensor for sensitive detection of miRNA-155 increased with increasing concentrations of miRNA-155. The calibration plots in Fig. 4b provided a distinguished linear relationship between the ECL intensity and the logarithm of miRNA-155 concentration in the range of 0.8 f. to 1.0 nM, with a correlation coefficient of 0.9965. The regression equation was $I_{ECL} = 18{,}729.6 + 1152.7 \lg c_{miRNA}$, moreover, the detection limit for miRNA-155 was 0.3 f. and at a signal-to-noise ratio of 3, demonstrating a satisfying method would be advantageous for the ultrasensitive determination of miRNA-155. This result was attributed to the high-selectivity decomposition of Hg^{2+} to RuMOFs, the recurrent utilization of target, the vast loading of DNA-I to functionalized RuMOFs. Table 1 compared the performance of our proposed miRNA biosensor with other works. As we expected, the detection limit of the proposed miRNA biosensor was comparable and even better than those of other reported methods in Table 1.

Specificity, stability and reproducibility of the proposed ECL biosensor

Specificity was a vital criterion for the designed biosensor since the interfering substances can influence the accuracy of the detection results. The response to the interfering substance was examined by testing the ECL intensity. The specificity of the proposed biosensor was evaluated by incubation with the blank solution (miRNA-155, 0 pM), noncomplementary DNA (nDNA, 100 pM), noncomplementary miRNA (nRNA, 100 pM), and single-

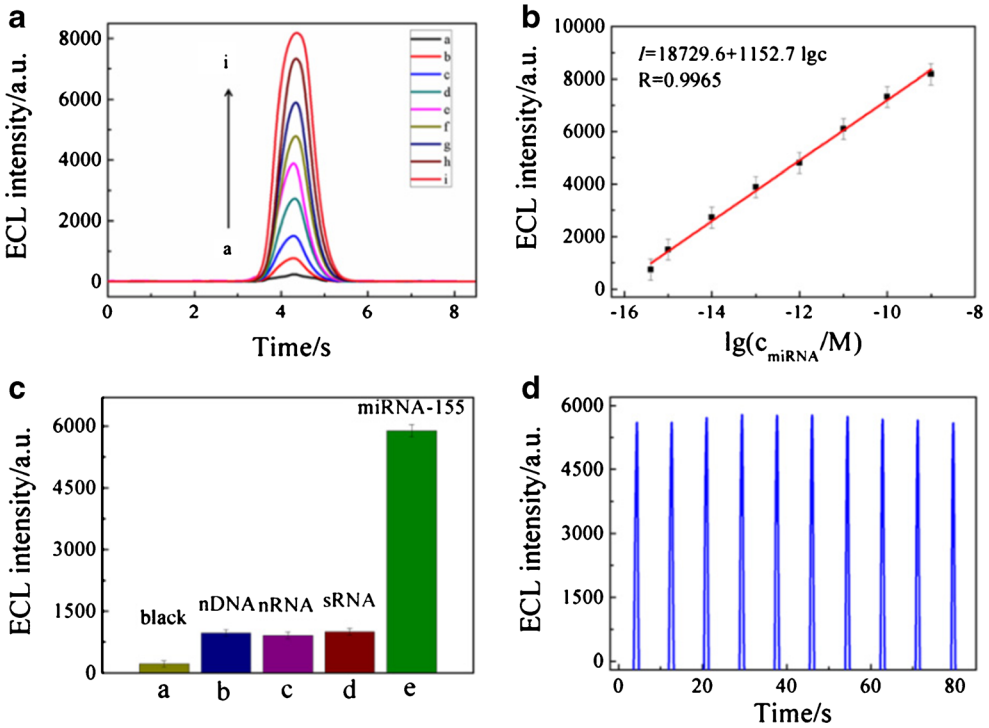

Fig. 4 **a** ECL measurements of miRNA-155 at different concentration: (a) 0 fM, (b) 0.8 fM, (c) 1 fM, (d) 10 fM, (e) 100 fM, (f) 1 pM, (g) 10 pM, (h) 100 pM, (i) 1 nM; **b** The linear relationship between the ECL signal and the concentration of miRNA-155; **c** Histograms for ECL intensity at equal conduction of different analyte. From a to e: using blank solution (0 f. miRNA-155), using noncomplementary DNA (nDNA, 100 pM), using noncomplementary miRNA (nRNA, 100 pM), using single-base difference miRNA (sRNA, 100 pM) and using miRNA-155 (10 pM); **d** ECL emission under continuous cyclic for 10 cycles at a scan rate of 200 mV·S^{-1} provide that the concentration of miRNA-155 was 10 pM. All the ECL measurements were in PBS (0.1 M, pH 7.0) containing TPA (1.0×10^{-3} M) (1:2). The potential was cycled within the window from 0 to 1.25 V with a scan rate of 200 mV·S^{-1}. The excitation wavelength is 425 nm

Table 1 Analytical performance compared with other works for miRNA detection

analytical method[a]	linear range	detection limit	materials[b]	Type of miRNA	reference
DPV	1.0 fM-0.1 nM	0.64 fM	AgNPs	miRNA-199a	[29]
CA	10 fM-5 pM	3 pM	AuNPs	miRNA-21	[30]
FL	1 f. - 50 pM	1.04 fM	DNA strand	miRNA-21	[31]
CL	10 pM-100 nM	0.69 pM	T7 exonuclease	miRNA-21	[32]
ECL	40 f. - 1.0 pM	20 fM	Nafion; Carbon	let-7a	[33]
ECL	0.8 fM-1 nM	0.3 fM	AuNPs@RuMOFs	miRNA-155	This work

[a] DPV: differential pulse voltammetry; CA: chronoamperometry; FL: fluorescence; CL: colorimetric; ECL: electrochemiluminescence

[b] NPs: nanoparticles; RuMOFs: tris(bipyridine)ruthenium(II) functionalized metal organic framework materials

base difference miRNA (sRNA, 100 pM), perfect complementary sequence (miRNA-155, 10 pM), respectively. Analyzed from the testing results with four parallel determinations under identical experimental conditions in Fig. 4c, it was obviously that the proposed biosensor exhibited negligible interference to target with an excess (10-fold) amount of nontarget analytes (nDNA, nRNA, and sRNA). Hence, the proposed biosensor actually owned satisfactory specificity. As shown in Fig. 4d, ECL emission originated from the RuMOFs was nearly consistent and hold a constant as well as ECL intensity observed merely had a mild decreased in spite of suffering several cycles, indicating the remarkable stability of this biosensor entirely. The reproducibility of the biosensor was evaluated by using the relative standard deviation (RSD) of the intra-assays and inter-assays. Three different concentrations of miRNA-155 standard solution (including 50.0 fM, 500.0 f. and 5.0 pM miRNA-155) were used as examples, and each RSD represented the average value of six assays on the same batch of the sensing device. It was gained from experimental results that the RSD values of the intra-assay were 4.6%, 6.2%, and 4.0% at 50.0 fM, 500.0 f. and 5.0 pM miRNA-155, whereas the RSD values of the inter-assay using different batches of sensing device were 6.4%, 3.4%, and 4.8% at 50.0 fM, 500.0 f. and 5.0 pM miRNA-155, respectively. Thus, the reproducibility of the assay was satisfied. These results together gave solid evidence that the proposed biosensor exhibited excellent ECL behavior.

Table 2 Determination of miRNA-155 spiked with different concentrations of miRNA in human serum ($n = 3$) by using the proposed biosensor

Sample	Added(M)	Found(M)	RSD(%)	Recovery(%)
1	2×10^{-15}	1.94×10^{-15}	3.48	97.17
2	2×10^{-14}	1.97×10^{-14}	4.12	98.81
3	2×10^{-13}	2.01×10^{-13}	2.21	100.65
4	2×10^{-12}	1.95×10^{-12}	3.96	97.85

Application in real sample

In order to evaluate the applicability and reliability of the proposed method for detecting real samples, we collected healthy human serum specimens from Shandong Tumor Hospital, China. Firstly, healthy human serum was 10-fold diluted. Then, different concentrations of miRNA-155 were added to above serum with the purpose of detecting the reliability of proposed biosensor. The proposed method showed acceptable feasibility to detect miRNA-155 in human serum. The results of determinations and recovery tests were shown in Table 2, showing acceptable results with relative standard deviation less than 4.12% for miRNA-155 detection and recoveries between 97.17% and 100.65% for the miRNA-155 recovery experiment. Satisfactory results were achieved, which proved the potentiality of this experimental method for practical applications with high sensitivity and selectivity.

Conclusions

An Electrochemiluminescence biosensor is achieved for the detection of miRNA-155 by combining target recycling process with disassembly of RuMOF. It is worth pointing that the I-RuMOFs-conjugates were linked on the surface of electrode by hybridizing with capture probes (H2). RuMOFs are not only used as nanocarriers to immobilize DNA-I, but also as luminescent materials for signal reporting. In addition, target recycling process tremendously promoted the signal amplification. This novel design of the biosensor provided a relatively low detection limit of 0.3 f. for miRNA-155. Compared with the other electrochemiluminescence detection methods, the biosensor illustrated a high sensitivity detection and a wide range of linearity for miRNA-155. Therefore, this method provides a pathway for miRNAs detection in clinical applications and opens up new opportunities for other analyte detection.

Acknowledgements This work was financially supported by the National Natural Science Foundation of China (21575051, 21775055, 21501090), 111 Project of International Corporation on Advanced Cement-based Materials (No. D17001) and the program of Taishan Scholars.

Compliance with ethical standards The author(s) declare that they have no competing interests.

References

1. Arner P, Kulyte A (2015) MicroRNA regulatory networks in human adipose tissue and obesity. Nat Rev Endocrinol 11:276–288
2. Wronska A, Kurkowska-Jastrzebska I, Santulli G (2015) Application of microRNAs in diagnosis and treatment of cardiovascular disease. Acta Physiol 213:60–83
3. Donnem T, Eklo K, Berg T, Sorbye SW, Lonvik K, Al-Saad S (2011) Prognostic impact of miR-155 in non-small cell lung cancer evaluated by in situ hybridization. J Transl Med 9:6
4. Nelson PT, Baldwin DA, Scearce LM, Oberholtzer JC, Tobias JM (2004) Mourelatos microarray-based, high-throughput gene expression profiling of microRNAs. Nat Methods 1(2):155–161
5. Kadimisetty K, Malla S, Sardesai NP, Joshi AA, Faria RC, Lee NH (2015) Automated multiplexed ECL immunoarrays for cancer biomarker proteins. Anal Chem 87:4472–4478
6. Ge SG, Lan FF, Liang LL, Ren N, Li L, Liu HY (2017) Ultrasensitive photoelectrochemical biosensing of cell surface N-glycan expression based on the enhancement of nanogold-assembled mesoporous silica amplified by graphene quantum dots and hybridization chain reaction. ACS Appl Mater Inter 9:6670–6678
7. Liang LL, Lan FF, Ge SG, Yu JH, Ren N, Yan M (2017) Metal-enhanced ratiometric fluorescence/naked eye bimodal biosensor for lead ions analysis with bifunctional nanocomposite probes. Anal Chem 89:3597–3605
8. Shen W, Deng HM, Ren YQ, Gao ZQ (2013) A real-time colorimetric assay for label-free detection of microRNAs down to sub-femtomolar levels. Chem Commun 49:4959–4961
9. Parshetti GK, Lin FH, Doong RA (2013) Sensitive amperometric immunosensor for α-fetoprotein detection based on multifunctional dumbbell-like au-Fe_3O_4 heterostructures. Sens Actuat B chem 186: 34–43
10. Lin DJ, Wu J, Wang M, Yan F, Ju HX (2012) Triple signal amplification of graphene film, polybead carried gold nanoparticles as tracing tag and silver deposition for ultrasensitive electrochemical immunosensing. Anal Chem 84:3662–3668
11. Tarn D, Ashley CE, Xue M, Carnes EC, Zink JI, Brinker CJ (2013) Mesoporous silica nanoparticle nanocarriers: biofunctionality and biocompatibility. Accounts Chem Res 46:792–801
12. Akter R, Rahman MA, Rhee CK (2012) Amplified electrochemical detection of a cancer biomarker by enhanced precipitation using horseradish peroxidase attached on carbon nanotubes. Anal Chem 84:6407–6415
13. Du D, Zou ZX, Shin YS, Wang J, Wu H, Engelhard MH (2010) Sensitive immunosensor for cancer biomarker based on dual signal amplification strategy of graphene sheets and multienzyme functionalized carbon nanospheres. Anal Chem 82:2989–2995
14. Miao W, Choi JP, Bard AJ (2002) Electrogenerated chemiluminescence: the Tris(2,2′-bipyridine)ruthenium(II), $(Ru(bpy)_3^{2+})$/tri-n-propylamine (TPrA) system revisited a new route involving $TPrA^{\bullet+}$ cation radicals. J Am Chem Soc 124:14478–14485
15. Ogawa M, Nakamura T, Mori JI, Kuroda K (2000) Luminescence of Tris(2,2′-bipyridine)ruthenium(II) cations ($[Ru(bpy)_3]^{2+}$) adsorbed in mesoporous silica. J Phys Chem C B 104:8554–8556
16. Wang WJ, Yuan DQ (2014) Mesoporous carbon originated from non-permanent porous MOFs for gas storage and $CO_{(2)}/CH_{(4)}$ separation. Sci Rep 4:5711
17. Nunes GG, Seisenbaeva GA, Kessler VG (2011) Crystal engineering of nanomorphology for complex oxide materials via thermal decomposition of metal-organic frameworks. Cryst Growth Des 11:1238–1243
18. Tan LL, Song N, Zhang XA, Li HW, Wang B, Yang YW (2016) Ca^{2+}, pH and thermo triple-responsive mechanized Zr-based MOFs for on-command drug release in bone diseases. J Mater Chem B 4:135–140
19. Wu MS, He LJ, Xu JJ, Chen HY (2014) RuSi@$Ru(bpy)_3^{2+}$/au@Ag_2S nanoparticles electrochemiluminescence resonance energy transfer system for sensitive DNA detection. Anal Chem 86: 4559–4565
20. Li LL, Liu HY, Shen YY, Zhang JR, Zhu JJ (2011) Electrogenerated chemiluminescence of au nanoclusters for the detection of dopamine. Anal Chem 83:661–665
21. Gu WL, Deng X, Gu XX, Jia XF, Lou BH, Zhang XW (2015) Stabilized, superparamagnetic functionalized graphene/Fe_3O_4@au nanocomposites for a magnetically-controlled solid-state electrochemiluminescence biosensing application. Anal Chem 87: 1876–1881
22. Saha K, Agasti SS, Kim C, Li X, Rotello VM (2012) Gold nanoparticles in chemical and biological sensing. Chem Rev 112:2739–2779
23. Lin XM, Luo FQ, Zheng LY, Gao GM, Chi YW (2015) Fast, sensitive, and selective ion-triggered disassembly and release based on tris(bipyridine)ruthenium(II)-functionalized metal-organic frameworks. Anal Chem 87:4864–4870
24. Li CX, Li YX, Xu X, Wang XY, Chen Y, Yang XD (2014) Fast and quantitative differentiation of single-base mismatched DNA by initial reaction rate of catalytic hairpin assembly. Biosens Bioelectron 60:57–63
25. Liu SF, Wang Y, Ming JJ, Lin Y, Cheng CB, Li F (2013) Enzyme-free and ultrasensitive electrochemical detection of nucleic acids by target catalyzed hairpin assembly followed with hybridization chain reaction. Biosens Bioelectron 49:472–477
26. Zhang DY, Chen SX, Yin P (2012) Optimizing the specificity of nucleic acid hybridization. Nat Chem 4:208–214
27. Zheng AX, Wang JR, Li J, Song XR, Chen GN, Yang HH (2012) Enzyme-free fluorescence aptasensor for amplification detection of human thrombin via target-catalyzed hairpin assembly. Biosens Bioelectron 36:217–221
28. Jiang Y, Li B, Milligan JN, Bhadra S, Ellington AD (2013) Real-time detection of isothermal amplification reactions with thermostable catalytic hairpin assembly. J Am Chem Soc 135:7430–7433
29. Yang CY, Shi K, Dou BT, Xiang Y, Chai YQ, Yuan R (2015) In situ DNA-templated synthesis of silver nanoclusters for ultrasensitive and label-free electrochemical detection of microRNA. ACS Appl Mater Inter 7:1188–1193
30. Liu L, Xia N, Liu HP, Kang X, Liu XS, Xue C (2014) Highly sensitive and label-free electrochemical detection of microRNAs based on triple signal amplification of multifunctional gold nanoparticles, enzymes and redox-cycling reaction. Biosens Bioelectron 53:399–405
31. Zhou YL, Li BC, Wang MH, Wang J, Yin HS, Ai SY (2017) Fluorometric determination of microRNA based on strand displacement amplification and rolling circle amplification. Microchim Acta 184:4359–4365
32. Sang Y, Xu YJ, Xu LL, Cheng W, Li XM, Wu JL, Ding SJ (2017) Colorimetric and visual determination of microRNA via cycling signal amplification using T7 exonuclease. Microchim Acta 184: 2465–2471
33. Xiong HT, Zheng XW (2017) Electrochemiluminescence based determination of micro-RNA using target-guided assembly of gold nanoparticles on an electrode modified with Nafion, carbon nanotubes and polyvinylpyrrolidone. Microchim Acta 184:1781–1789